PAPER

Helicity dependent Wigner phase shift for photoionization in a circularly polarized laser field

To cite this article: Run Wang *et al* 2022 *J. Phys. B: At. Mol. Opt. Phys.* **55** 115001

View the article online for updates and enhancements.

You may also like

IOP ebooks™

Bringing together innovative digital publishing with leading authors from the global scientific community.

Start exploring the collection−download the first chapter of every title for free.

Helicity dependent Wigner phase shift for photoionization in a circularly polarized laser field

Run Wang[1]**, Qingbin Zhang**[1,*] ⬛**, Chuanpeng Cao**[1]**, Min Li**[1] ⬛**, Kunlong Liu**[1,*] **and Peixiang Lu**[1,2,3]

[1] School of Physics and Wuhan National Laboratory for Optoelectronics,
Huazhong University of Science and Technology, Wuhan 430074, People's Republic of China
[2] Hubei Key Laboratory of Optical Information and Pattern Recognition, Wuhan Institute of Technology,
Wuhan 430205, People's Republic of China
[3] Optics Valley Laboratory, Hubei 430074, People's Republic of China

E-mail: zhangqingbin@hust.edu.cn and liukunlong@hust.edu.cn

CrossMark

Abstract

The sensitivity of strong-field ionization to atomic orbital helicity has attracted much attention from physicists, due to its potential application in attosecond spectroscopy and spintronics. In order to intuitively observe the physical mechanisms of helicity-dependent ionization rates during photoionization, the concept of the Wigner phase can be used to characterize the different interactions between the rotating electrons and the Coulomb potential. Here, we find that in both one- and three-photon ionization schemes, the electrons liberated more easily by the circularly polarized laser field suffer less influence of the Coulomb potential during the propagation and then accumulate less Winger phase. This result indicates that the strength of the interaction between the rotating electrons and the Coulomb potential can explain the helicity-dependent ionization for different ionization mechanisms universally, which is also supported by our classical ensemble analysis. Our work provides an intuitive perspective towards the physics picture of ionization propensity rules.

Keywords: atomic orbital helicity, Wigner phase shift, photoionization

(Some figures may appear in colour only in the online journal)

1. Introduction

In a circularly polarized laser field, the sensitivity of ionization rates to atomic orbital helicity (the sign of magnetic quantum number) is one of the key signatures of strong-field ionization. It has been indicated that electrons counter-rotating with respect to the laser field can be liberated more easily than co-rotating electrons [1–3]. On the other hand, it is well known that circularly polarized light does preferentially ionize co-rotating electrons in one-photon ionization or the ionization of circular Rydberg states [4, 5]. This

sensitivity of ionization is a crucial element in the generation of spin-polarized electrons, which has many practical applications like studying chiral molecules [6, 7], magnetic materials [8] and spintronics [9]. Recently, these various propensity rules in different ionization schemes had been understood from a simple classical analogy by Askeland *et al* [10] and Wu *et al* [11]. It is superficially explained that if the electrons interact strongly with the nucleus, the catalytic of the nucleus is more pronounced, causing more ionization. However, how to quantitatively demonstrate the different interactions between the rotating electrons and the Coulomb potential and find the physical principle to unify the various ionization propensity rules, is a most interesting but not discussed issue.

---

* Authors to whom any correspondence should be addressed.

All these diverse Coulomb interactions are expected to leave different imprints on the phase of the photoelectron wave packet. In scattering theory [12–14], the phase of the outgoing electron wave packet (EWP) is a direct consequence of the interaction of the photoelectron and the scattering potential. The scattering delay (also-called Wigner delay) represents the delay between an electron scattering in a given Coulomb potential and a reference potential ($V = 0$). Namely, the effect of the interaction potential on the released EWP is expressed as either a phase or delay. This scattering physics is intrinsic to the various quantum systems like atoms, molecules, and solids [15–18], and can provide detailed information on electronic correlations [19], potential [20], and orbital shapes [21]. Such Wigner delay had been used to observe the physics dynamics of the ionization process, for instance, quantifying the time-resolved dynamics in the tunnel ionization of H_2 molecules [22], revealing the multi-electronic effect in photoionization of chiral molecules [23], and probing scattering potential in the small asymmetric molecular system [24, 25]. Hence, we can use this Wigner phase as a measurement tool to observe the different interactions between the rotating electrons and the Coulomb potential in the cases of various ionization propensity rules.

Generally, the dynamics of the photoionization are encoded in the phase of the escaping EWP. Traditionally, this phase cannot be directly observed in the frequency domain, but can be retrieved by attosecond streaking [26] and reconstruction of attosecond beating by interference of two-photon transition (RABBITT) [27, 28]. These methods have been extended to the above-threshold ionization (ATI) regime for the phase measurements of ATI electrons by employing the two-color laser field in a combination of a strong ionizing field and a weak probing field at half the ionizing laser frequency in reference [29]. Up to now, this photoelectron interferometry has been widely applied in ATI, like to experimentally measure the relative time delays among the resonant ionization with the orthogonal [30] or parallel [31] two-color laser fields. These methods are conceptually similar, where the phase properties of the photoemission process are both extracted from the oscillation signal of two-path interference.

In this paper, we theoretically investigate the differential Wigner phase shifts between the p_+ and p_- orbitals of xenon atom by solving the two-dimensional time-dependent Schrödinger equation (TDSE). We achieve this by calculating the photoelectron momentum distributions (PMDs) as a function of time delay between a strong left circularly polarized (LCP) field and a week linearly polarized field. We tactfully design one- and three-photon ionization schemes and observe negative and positive differential Wigner phase shifts between $p_\pm$ orbitals, respectively, indicating that the Wigner phase shift in circularly polarized laser field depends on atomic orbital helicity. On the other hand, we adopt a classical ensemble scheme for providing the supporting calculations. By analyzing the electronic trajectories, we observe that the co-rotating electrons prefer to obtain energy from the laser field when moving away from the nucleus, especially in one-photon ionization. However, as the laser wavelength increases to three-photon ionization, the period for obtaining energy decreases

for the co-rotating case leading to a reversal of ionization propensity rules. Atomic units are used throughout unless stated otherwise.

2. Theory and models

To calculate the photoelectron momentum distributions (PMDs) for the $p_\pm$ orbitals in xenon [32, 33], we numerically solve the two-dimensional TDSE with the single-active electron approximation in two-color laser field,

$$i\partial\psi(\mathbf{r}, t)/\partial t = [H_0 + V_E(\mathbf{r}, t)]\psi(\mathbf{r}, t). \tag{1}$$

$H_0 = T + V_0(\mathbf{r})$ is the time-independent Hamiltonian, where $T = -\nabla^2/2$ is the kinetic energy operator and $V_0(\mathbf{r})$ is the atom potential. $\psi(\mathbf{r}, t)$ is the time-dependent wavefunction. $V_E(\mathbf{r}, t) = -\mathbf{E}(t) \cdot \mathbf{r}$ is the laser-electron interaction potential under dipole approximation in length gauge. The laser field $\mathbf{E}(t)$ is expressed by
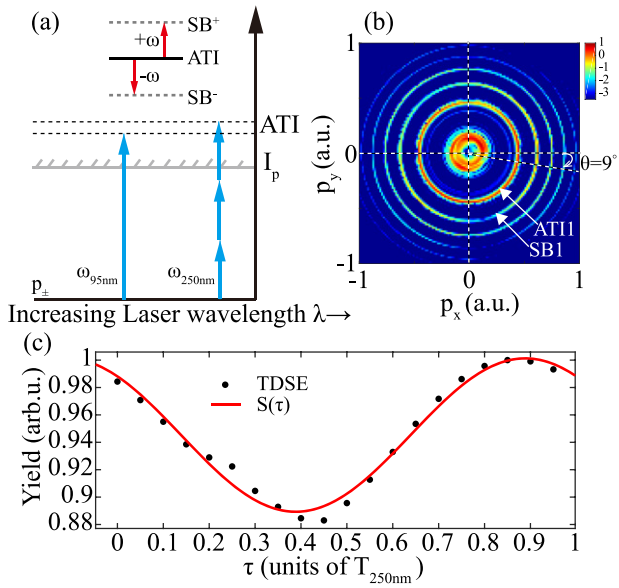
$$\mathbf{E}(t) = \mathbf{E}_1(t) + \mathbf{E}_2(t + \tau), \tag{2}$$

where $\mathbf{E}_i(t) = E_0^i f_i(t)[\cos(\omega_i t)\mathbf{e_x} + \varepsilon_i \sin(\omega_i t)\mathbf{e_y}]$, and τ is the time delay between two laser fields. For the ith pulse ($i = 1, 2$), its polarization $\varepsilon_1 = \pm 1$ for the circularly polarized field and $\varepsilon_2 = 0$ for the linearly polarized field. The carrier-envelope phases of the two pulses are both zero. E_0^i is its field amplitude, $f_i(t) = \sin^2(\pi t/T_i)$ is its temporal envelope, and $T_i = N_i(2\pi/\omega_i)$ is its duration with N_i being the number of cycles. The TDSE is solved by utilizing the split-step Fourier method [34], where the time step is 0.04 a.u., and the spatial discretization is 0.2 a.u. with the dimension size of 400 a.u..

Furthermore, the classical approach may facilitate the interpretation of the results from the quantum-mechanical calculations, and provide further insight into the underlying physical mechanisms [35, 36]. It has been proved that the classical ensemble model can be applied with great care to describe strong-field laser-atom interactions [37, 38]. The electronic motion can be described by the classical time-dependent Newton equation as: $\partial^2\mathbf{r}/\partial t^2 = -\nabla V(\mathbf{r}) - \mathbf{E}(t)$, where $\mathbf{r}$ is the coordinate of the electron and the atomic potential of xenon $V_0(\mathbf{r}) = -1/\sqrt{\mathbf{r}^2 + a^2}$ [39]. To mimic the initial states with angular momenta $L = \pm 1$, we first randomly select the electronic position x and y from a microcanonical ensemble [40] to determine the total potential energy of the electrons, then the electron kinetic energy E_k can be obtained by the energy conservation. We combine equations $\mathbf{L} = \mathbf{r} \times \mathbf{p}$ and $E_k = (p_x^2 + p_y^2)/2$, to determine the initial momenta of the electrons. With these initial conditions, we solve the Newton equation for 4×10^5 classical trajectories and obtain the ionization probability P_{ion} by taking the ratio between the number of ionized electrons with energy more than zero and the total number of electronic trajectories.

In the absence of laser field, the time evolution of a non-relativistic photoelectron is described by the time-independent Schrödinger equation [41],

$$H_0\psi_\alpha(\mathbf{r}) = \epsilon_\alpha\psi_\alpha(\mathbf{r}), \tag{3}$$

J. Phys. B: At. Mol. Opt. Phys. **55** (2022) 115001

R Wang *et al*

Figure 1. (a) Ionization schemes for the $p_\pm$ orbitals in xenon atom. The ATI is induced by a strong LCP laser field (blue arrows). The inset describes in the presence of a week linearly polarized laser field, new peaks, called sidebands, generate from the ATI peak by absorbing or emitting an additional photon (red arrows). (b) The photoelectron momentum distribution at zero time delay in the three-photon ionization scheme for the p_+ orbital. The first order of ATI peak (ATI1) and the first sideband is denoted by the white arrows, respectively. (c) The oscillation signal of ATI1 in three-photon ionization scheme for the p_+ orbital in the $0°$–$9°$ slice as a function of τ fitted by a cosine form $S(\tau)$ (red curves).

Figure 2. The differential Wigner phase shifts $\Delta\phi_{\text{Wigner}}^{p/m}$ between the p_+ and p_- orbitals as a function of the photoelectron ejection angle θ (°), (a) in three-photon ionization and (b) in one-photon ionization.

where ϵ_α is the eigenvalue of the solution and $\psi_\alpha(\mathbf{r})$ is labelled by a set of quantum numbers α ($\alpha = [n, \lambda, m]$). In spherical potential with states on a spherical basis, the one-dimensional Schrödinger equation for effective radial states $\mu_{n,\lambda}(r)$ ($r > 0$) is written as $[T + V_0(r)]\mu_{n,\lambda}(r) = \epsilon_\alpha\mu_{n,\lambda}(r)$. The propagation of a photoelectron wave packet is governed by the way in which the phases of continuum states $\mu_{n,\lambda}(r)$ vary as a function of energy ϵ ($\epsilon > 0$). Considering that the Wentzel–Kramers–Brillouin (WKB) approximation is well suited for studying continuum states within a semi-classical framework [42]. For the potential which vanishes at infinity i.e. $\lim_{r\to\infty} V_0(r) = 0$, the radial wavefunction is taken to be
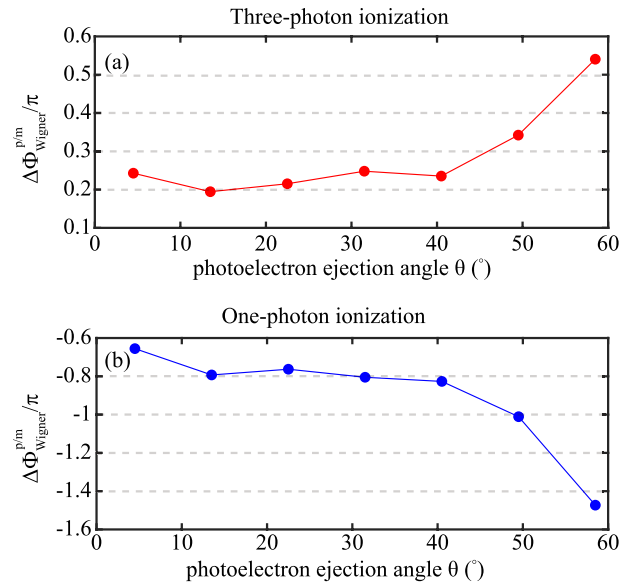
$$u_\epsilon(r) \propto \xi\{\exp[i\phi(\epsilon, r)]\} = \sin[\phi(\epsilon, r)], \tag{4}$$

inserting this radial wavefunction into the equation (3) leads to a differential equation for the phase of the state:

$$-i\frac{\partial^2 \phi}{\partial r^2} + \left(\frac{\partial \phi}{\partial r}\right)^2 = \epsilon - V_0(r). \tag{5}$$

Furthermore, assuming that the local momentum of photoelectron varies slowly, $|p(r)| \equiv |\partial\phi/\partial r| \gg (\partial^2\phi/\partial r^2)^{1/2}$, the above equation can be simplified,

$$\frac{\partial\phi}{\partial r} = \sqrt{2\,m\,[\epsilon - V_0(r)]}, \tag{6}$$

and then integrated,

$$\phi(\epsilon, r, r_0) = \int_{r_0}^{r} dr' \sqrt{2\,m\,[\epsilon - V_0(r')]}, \tag{7}$$

where ϵ is the energy of the electron, r_0 is where the electron 'starts', and $V_0(r)$ is the atomic potential determined by the classical trajectories in the absence of the laser field. We can see that the electron at a given energy is classically allowed to pass through the potential and acquires a quantum phase which depends on the potential $V_0(r)$ and the starting position r_0. If the electron suffers less influence of the Coulomb potential, the phase the electron accumulates during the propagation is smaller.

3. Results and discussion

We present the basic concepts of photoelectron interferometry for analyzing the direct photoionization dynamics described in figure 1. Firstly, the electrons from the $p_\pm$ orbitals are ionized by a strong LCP laser field (counterclockwise, $\varepsilon_1 = +1$, $\omega_1 = 2\omega$) by absorbing n-photon. The energy of the ATI peak follows $E_k = n\omega - I_p - U_p$, where n is the number of photons absorbed in the ionization process, I_p is the ionization potential, and $U_p = I/(2\omega)^2$ is the ponderomotive energy. Here, the energy of the first ATI peak is at 0.92 eV and 2.78 eV in one- and three-photon ionization, respectively. Next, we probe this ATI process using a week linearly polarized laser field ($\varepsilon_2 = 0$), at half the frequency of the LCP laser field ($\omega_2 = \omega$). Sideband peaks appear in the ATI spectrum, at energies that correspond to the absorption or emission of a probe photon. Due to the interference of these two paths, the ATI peaks have a cosinoidal modulation with respect to the relative time delay τ between the pump and probe laser fields, similar to RABBIT analysis [27, 28]. The probability of the ATI peaks
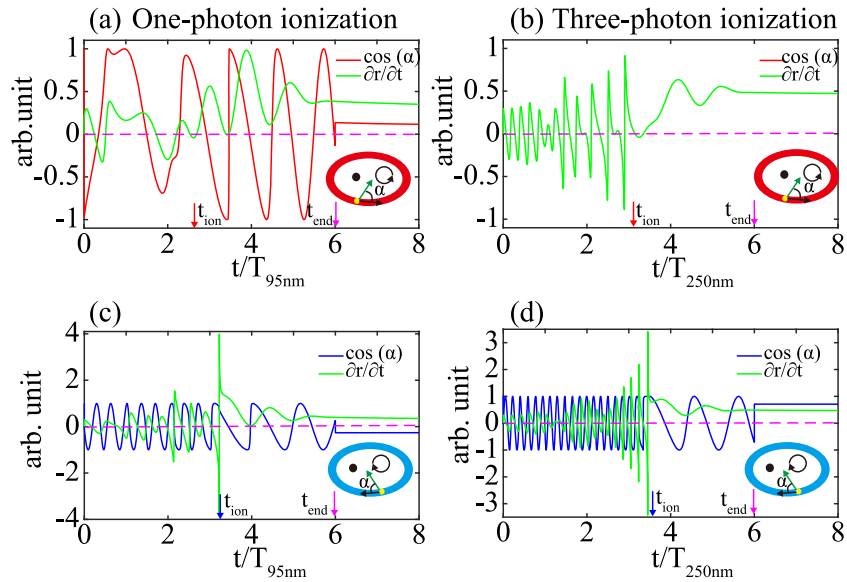
Figure 3. The cosine of the angle α between the force of the laser field on the electron and its displacement, and the velocity ($\partial r/\partial t$) as a function of time, (a) and (b) for the p_+ orbital and (c) and (d) for the p_- orbital. We stipulate that the energy reaches zero at t_{ion} defined as the ionization moment marked by the vertical arrows. The insets show the schematic diagrams of the relative movement between the laser field and the electron. The green arrow and the black arrow represent the direction of the force of the laser field (F) and the electron displacement (S), respectively. The circle with an arrow represents the direction of the rotating electron. The LCP laser field is at 250 nm with the intensity of 4.5×10^{14} W cm^{-2} and $N = 6$ in three-photon ionization, and at 95 nm with the intensity of 6.8×10^{15} W cm^{-2} and $N = 6$ in one-photon ionization. After the pulse end (at t_{end} marked by the purple arrows), the electron is in free propagation with the duration of two cycles.

modulates as

$$S_n = \alpha + \beta \cos[2\omega\tau - \Delta\phi_{\text{light}} - \Delta\phi_{\text{Wigner}} - \Delta\phi_{\text{cc}}]. \quad (8)$$

The total phase shift $\Delta\phi = \Delta\phi_{\text{light}} + \Delta\phi_{\text{Wigner}} + \Delta\phi_{\text{cc}}$, where $\Delta\phi_{\text{light}}$ is the phase difference between the two laser fields. The Wigner phase shift $\Delta\phi_{\text{Wigner}}$ is the phase shift between the ionized electron scattering in the atomic potential, and a reference potential [13]. Moreover, the weak probe field introduces an additional phase shift $\Delta\phi_{\text{cc}}$, by inducing continuum–continuum transitions of the electrons from the main ATI peaks to the sidebands. Here, the total phase shift can be converted into the time delay by the relation of $\tau = \Delta\phi/2\omega$.

By analyzing the oscillation signal of the first ATI peak, we extract the differential phase shifts between the electrons emitted from the p_+ and p_- orbitals, where $\Delta\phi^{p/m} = \Delta\phi^p - \Delta\phi^m$. This procedure naturally eliminates $\Delta\phi_{\text{light}}$, which is strictly common for the same laser fields. On the other hand, we can selectively render the equality of $\Delta\phi_{\text{cc}}$ for the $p_\pm$ orbitals by using a linearly polarized laser field. In this case, $\Delta\phi_{\text{cc}}^{p/m} = 0$, and $\Delta\phi^{p/m} = \Delta\phi_{\text{Wigner}}^{p/m}$. The differential Wigner phase shift $\Delta\phi_{\text{Wigner}}^{p/m}$ has been investigated in two kinds of ionization schemes described in figure 1(a). We tactfully design the one- and three-photon ionization schemes to compare Wigner phase shifts in the cases of opposite ionization propensity rules, where the photoelectrons for the $p_\pm$ orbitals have the same energy but different yields. Here, the one-photon ionization is induced by a strong LCP laser field at 95 nm with the intensity of 6×10^{13} W cm^{-2} and probed by a week linearly polarized laser field at 190 nm with the intensity of 2.4×10^{12} W cm^{-2} and $N_2 = 60$. In the three-photon ionization scheme, we

employ a strong LCP laser field of 250 nm at 4×10^{13} W cm^{-2} and a week linearly polarized laser field of 500 nm at 1.6×10^{12} W cm^{-2} and $N_2 = 30$. In both ionization schemes the intensity ratio between the ionizing laser field and the probe laser field is $I_\omega/I_{2\omega} = 1/25$, which ensures that this technique is in a RABBIT-like regime and no higher-order phenomenon (4ω or higher orders) affects the phase measurements.

The $\Delta\phi_{\text{Wigner}}^{p/m}$ in two ionization schemes are calculated by integrating the photoelectron signal in slices of 9° around different ejection angles θ starting from the x-axis in figure 1(b). The photoelectron angular distribution composed of ATI peaks and sidebands appearing between the ATI comb. The energy interval between the neighboring ATI peaks are equal to the ionizing laser photon energy of 4.96 eV. The ATI peaks and sidebands is separated by the probe photon energy of 2.48 eV. The superposition of the LCP laser field and the linear polarized laser field produces an electric field that is stronger in the x-axis direction, which causes the amplitude modulation of the sideband oscillation signal is stronger near the laser polarization direction (x-axis). Hence, for electrons emitted beyond 60°, the signal is too low to extract reliable values. In order to extract the phase, the oscillation signal of the first ATI peak as a function of the time delay between the two laser fields is fitted with the four-parameter cosine formula $S(\tau) = \sigma + \beta \cos(2\omega\tau - \phi)$ shown in figure 1(c). We also analyze this signal by the Fourier transform, and find that these results are in good agreement.

The evolution of the differential Wigner phase shifts $\Delta\phi_{\text{Wigner}}^{p/m}$ with the photoelectron ejection angle is shown in figure 2. The positive $\Delta\phi_{\text{Wigner}}^{p/m}$ are observed in three-photon ionization shown in figure 2(a). For electrons emitted in the
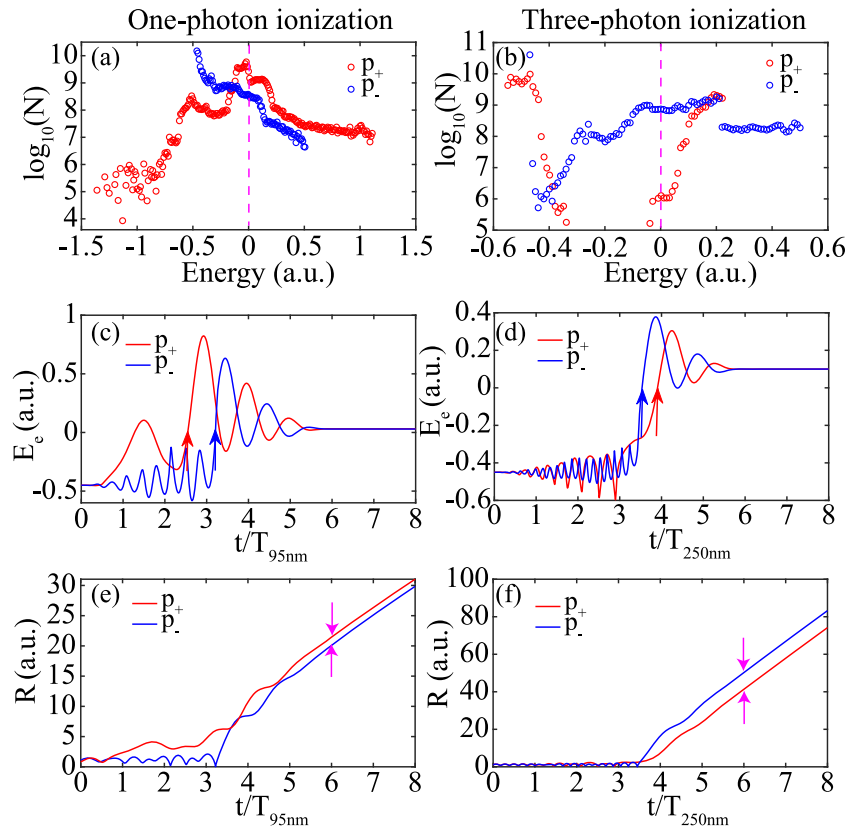
Figure 4. (a) and (b) Photoelectron energy spreading at the end of the laser field for the one- and three-photon ionization schemes, respectively. (c) and (d) The energy E_e (the potential energy plus the kinetic energy) of the ionized electron as a function of time. The colorful arrows represent the ionization moments t_{ion} where $E_e = 0$. (e) and (f) The distance R between the ionized electron and the nucleus as a function of time. The purple arrows represent the position at the end of the laser field.

$0°$–$9°$ slice, $\Delta\phi_{Wigner}^{p/m}$ reaches 0.24π radians. The differential Wigner phase shifts strongly vary with ejection angle and can reach a higher value of 0.54π radians when electrons are emitted away from the polarized axis of the probe light (x-axis). The co-rotating electrons (ionized from the p_+ orbital) have more Wigner phase shift than the counter-rotating electrons (ionized from the p_- orbital). On the contrary, in the one-photon ionization scheme, it is found the negative $\Delta\phi_{Wigner}^{p/m}$ ranging from -0.66π to -1.47π radians with the increasing ejection angle shown in figure 2(b), which means that the Wigner phase shift in the co-rotating case is smaller than that in the counter-rotating case. These results demonstrate that the Winger phase shift is sensitive to atomic orbital helicity in a circularly polarized laser field, due to the diverse interactions between the rotating electrons and the Coulomb potential.

We make supporting calculations by using a classical ensemble scheme. The results of the classical calculation are shown in figures 3 and 4. We calculate the cosine of the angle α and the velocity ($\partial r/\partial t$) of the electron as a function of time in figure 3. The angle α is between the force of the laser field F, and the electron's displacement S. The work done by the laser field on the electron is calculated by $W = FS\cos(\alpha)$, where the positive (negative) cosine represents positive (negative) work. We define the direction away from the nucleus as positive, corresponding to positive velocity ($\partial r/\partial t > 0$). The

evolution of the electron's motion with time can be divided into three stages. The first stage is that the electron oscillates around the nucleus before the ionization moment t_{ion} marked by vertical arrows in figure 3. Then the electron can escape from the nucleus and move away in the laser field. After the laser field end, the free electron continues to move away. In the first oscillating process, it can be seen that the electron can obtain or lose energy from the laser field shown in figure 3. In the co-rotating case, the $\cos(\alpha)$ and the velocity have the same sign, which means that the force of the laser field does the positive (negative) work when the electron moves away from (close to) the nucleus. On the contrary, in the counter-rotating case, the $\cos(\alpha)$ and the velocity have the opposite sign. Therefore, the force of the laser field does the positive work, when the electron moves close to the nucleus. The insets show schematic diagrams of these movements in figure 3. On the other hand, the period of doing work is longer in the co-rotating case than in the counter-rotating case, due to that the circularly polarized laser field slows down the co-rotating electrons and speeds up the counter-rotating electrons.

Based on the above analysis of the electron motion, we investigate the electronic trajectories to understand the physical origin of the propensity rules. Firstly, we discuss the classical calculations in the one-photon ionization scheme shown in the left panels of figure 4. It is shown that the co-rotating

case has a wider energy spreading and more high-energy electrons than the counter-rotating case as shown in figure 4(a). For one thing, the co-rotating electrons can lose ($W < 0$) or obtain ($W > 0$) energy from the laser field when moving close to or far away from the nucleus. Another critical element is the period of doing work by the laser field, where the longer the period is, the more energy the electron can obtain or lose from the laser field. It can be seen that this period is longer in the co-rotating case than in the counter-rotating case shown in figure 3(a). Consequently, the co-rotating electrons can be promoted into lower or higher energy states, which leads to wider energy spreading. However, in the counter-rotating case, the work done by the laser field in the opposite process can hamper the electrons promoting into higher or lower energy states, leading to narrow energy spreading. The corresponding ionization probability in the co-rotating case ($P_{ion} = 0.33$) is greater than that in the counter-rotating case ($P_{ion} = 0.05$). Furthermore, the co-rotating electron has more oscillation energy in the laser field after ionization than the counter-rotating electron when moving away from the nucleus shown in figure 4(c). Hence, the co-rotating electron can move farther before the end of laser field shown in figure 4(e) and then suffer less influence by the Coulomb potential. With the trajectories starting from the position marked by the vertical arrows in figure 4(e), the Wigner phase shift will be calculated by equation (7). It is obtained that the phase shift is 3.6 a.u. for the p_+ orbital and 3.9 a.u. for the p_- orbital. The differential phase shift between the $p_{\pm}$ orbitals is -0.3 a.u., indicating that the Wigner phase shift in the co-rotating case is smaller than that in the counter-rotating case.

As the laser wavelength increases, in three-photon ionization, the laser field rotates more slowly and dramatically reduces the effect on the electrons' rotation speed, especially for the co-rotating case resulting in a significantly shorter period of doing work shown in figure 3(b). In this case, the energy spreading of the co-rotating case becomes narrow, but the counter-rotating case has little impact. Figure 4(b) shows that the counter-rotating case has more high-energy electrons than the co-rotating case. We obtain the ionization probability of 0.19 for the co-rotating case and 0.35 for the counter-rotating case. Moreover, the counter-rotating electron has more oscillation energy in the second process and can move farther from the nucleus shown in figures 4(d) and (f). The calculated differential phase shift between the $p_{\pm}$ orbitals is 0.27 a.u., indicating that the Wigner phase shift of the co-rotating electron is more significant than that of the counter-rotating electron. As expected, these classical results can strongly support the quantum-mechanical calculations.

4. Conclusion

In summary, we calculate the differential Wigner phase shifts between the $p_{\pm}$ orbitals as a function of the ejection angle in a two-color laser field and find negative and positive differential Wigner phase shifts in the one- and three-photon ionization schemes, respectively. The reason is that the Wigner phase can

be used as a fingerprint of the diverse interactions between the rotating electrons and the Coulomb potential. It is indicated that the high ionization rate is associated with a small Wigner phase shift regardless of the ionization scheme. We also make supporting calculations by using a classical ensemble scheme. Analyzing the classical electron trajectories in both cases shows that in the case of high ionization probability, there are more high-energy electrons, which have more oscillation energy in the laser field and can move away from the nucleus to accumulate less Wigner phase. The inversion of ionization propensity rules from one- to three-photon ionization is caused by the rapidly decreasing period of doing work by the laser field with the increasing of laser wavelength in the co-rotating case. Our results provide an intuitive perspective towards the interaction between the rotating electrons and the Coulomb potential and open up a new avenue to experimentally observe the sensitivity of ionization to atomic orbital helicity. Our work provides a prospect for measuring photoelectron dynamics in atom, molecular and solid targets.

Data availability statement

The data that support the findings of this study are available upon reasonable request from the authors.

ORCID iDs

Qingbin Zhang ![ORCID] https://orcid.org/0000-0002-2277-7414
Min Li ![ORCID] https://orcid.org/0000-0001-7790-9739

References

[1] Barth I and Smirnova O 2011 Nonadiabatic tunneling in circularly polarized laser fields: physical picture and calculations *Phys. Rev.* A **84** 063415
[2] Herath T, Yan L, Lee S K and Li W 2012 Strong-field ionization rate depends on the sign of the magnetic quantum number *Phys. Rev. Lett.* **109** 043004
[3] Zhu X, Lan P, Liu K, Li Y, Liu X, Zhang Q, Barth I and Lu P 2016 Helicity sensitive enhancement of strong-field ionization in circularly polarized laser fields *Opt. Express* **24** 4196
[4] Rzazewski K and Piraux B 1993 Circular Rydberg orbits in circularly polarized microwave radiation *Phys. Rev.* A **47** R1612
[5] Zakrzewski J, Delande D, Gay J-C and Rzażewski K 1993 Ionization of highly excited hydrogen atoms by a circularly polarized microwave field *Phys. Rev.* A **47** R2468
[6] Böwering N, Lischke T, Schmidtke B, Müller N, Khalil T and Heinzmann U 2001 Asymmetry in photoelectron emission from chiral molecules induced by circularly polarized light *Phys. Rev. Lett.* **86** 1187

J. Phys. B: At. Mol. Opt. Phys. 55 (2022) 115001

R Wang *et al*

[7] Janssen M H M and Powis I 2014 Detecting chirality in molecules by imaging photoelectron circular dichroism *Phys. Chem. Chem. Phys.* **16** 856

[8] Stöhr J, Wu Y, Hermsmeier B D, Samant M G, Harp G R, Koranda S, Dunham D and Tonner B P 1993 Element-specific magnetic microscopy with circularly polarized x-rays *Science* **259** 658

[9] Žutić I, Fabian J and Sarma S D 2004 Spintronics: fundamentals and applications *Rev Mod. Phys.* **76** 323

[10] Askeland S, Sørngård S A, Pilskog I, Nepstad R and Førre M 2011 Stabilization of circular Rydberg atoms by circularly polarized infrared laser fields *Phys. Rev.* A **84** 033423

[11] Wu D, Guo F-M, Chen J-G, Wang J and Yang Y-J 2020 Ionization of an atom with different initial angular momenta in an intense circular polarized laser field *J. Phys. B: At. Mol. Opt. Phys.* **53** 235601

[12] Eisenbud L 1948 *The Formal Properties of Nuclear Collisions* (Princeton, NJ: Princeton University Press)

[13] Wigner E P 1955 Lower limit for the energy derivative of the scattering phase shift *Phys. Rev.* **98** 145

[14] Smith F T 1960 Lifetime matrix in collision theory *Phys. Rev.* **118** 349

[15] Ossiander M *et al* 2018 Absolute timing of the photoelectric effect *Nature* **561** 374

[16] Huppert M, Jordan I, Baykusheva D, von Conta A and Wörner H J 2016 Attosecond delays in molecular photoionization *Phys. Rev. Lett.* **117** 093001

[17] Palatchi C, Dahlström J M, Kheifets A S, Ivanov I A, Canaday D M, Agostini P and DiMauro L F 2014 Atomic delay in helium, neon, argon and krypton *J. Phys. B: At. Mol. Opt. Phys.* **47** 245003

[18] Sabbar M, Heuser S, Boge R, Lucchini M, Carette T, Lindroth E, Gallmann L, Cirelli C and Keller U 2015 Resonance effects in photoemission time delays *Phys. Rev. Lett.* **115** 133001

[19] Fano U 1961 Effects of configuration interaction on intensities and phase shifts *Phys. Rev.* **124** 1866

[20] Dehmer J L 1972 Evidence of effective potential barriers in the x-ray absorption spectra of molecules *J. Chem. Phys.* **56** 4496

[21] Cooper J W 1962 Photoionization from outer atomic subshells. A model study *Phys. Rev.* **128** 681

[22] Trabert D *et al* 2021 Angular dependence of the Wigner time delay upon tunnel ionization of H_2 *Nat. Commun.* **12** 1697

[23] Beaulieu S *et al* 2017 Attosecond-resolved photoionization of chiral molecules *Science* **358** 1288

[24] Hockett P, Frumker E, Villeneuve D M and Corkum P B 2016 Time delay in molecular photoionization *J. Phys. B: At. Mol. Opt. Phys.* **49** 095602

[25] Chacon A, Lein M and Ruiz C 2014 Asymmetry of Wigner's time delay in a small molecule *Phys. Rev.* A **89** 053427

[26] Itatani J, Quéré F, Yudin G L, Ivanov M Y, Krausz F and Corkum P B 2002 Attosecond streak camera *Phys. Rev. Lett.* **88** 173903

[27] Paul P M, Toma E S, Breger P, Mullot G, Augeé F, Balcou P, Muller H G and Agostini P 2001 Observation of a train of attosecond pulses from high harmonic generation *Science* **292** 1689

[28] Dahlström J M, Guénot D, Klünder K, Gisselbrecht M, Mauritsson J, L'Huillier A, Maquet A and Taïeb R 2013 Theory of attosecond delays in laser-assisted photoionization *Chem. Phys.* **414** 53–64

[29] Zipp L J, Natan A and Bucksbaum P H 2014 Probing electron delays in above-threshold ionization *Optica* **1** 361

[30] Gong X *et al* 2017 Energy-resolved ultrashort delays of photoelectron emission clocked by orthogonal two-color laser fields *Phys. Rev. Lett.* **118** 143203

[31] Ge P, Han M, Liu M M, Gong Q and Liu Y 2018 Probing time delays and coherent imaging of multiphoton resonant ionization *Phys. Rev.* A **98** 013409

[32] Bauch S and Bonitz M 2008 Angular distributions of atomic photoelectrons produced in the UV and XUV regimes *Phys. Rev.* A **78** 043403

[33] Protopapas M, Keitel C H and Knight P L 1997 Atomic physics with super-high intensity lasers *Rep. Prog. Phys.* **60** 389–486

[34] Feit M D, Fleck J A and Steiger A 1982 Solution of the Schrödinger equation by a spectral method *J. Comput. Phys.* **47** 412

[35] Farrelly D and Uzer T 1995 Ionization mechanism of Rydberg atoms in a circularly polarized microwave field *Phys. Rev. Lett.* **74** 1720

[36] Uzer T, Lee E and Farrelly D 1998 Ionization of Rydberg atoms by Coriolis forces *Phys. Rev.* A **58** 4761

[37] Hansen J, Lu J, Madsen L and Nilsen H 2001 Ionization and excitation dynamics of H(1s) in short intense laser pulses *Phys. Rev.* A **64** 033418

[38] Nilsen H M, Madsen L and Hansen J 2002 Ionization and excitation dynamics of H(1s) in short intense laser pulses. II *Phys. Rev.* A **66** 025402

[39] Huang C, Liao Q, Zhou Y and Lu P 2010 Role of Coulomb focusing on the electron transverse momentum of above-threshold ionization *Opt. Express* **18** 14293–300

[40] Reinhold C O and Falcón C A 1986 Classical ionization and charge-transfer cross sections for $H^+ + He$ and $H^+ + Li^+$ collisions with consideration of model interactions *Phys. Rev.* A **33** 3859

[41] Dahlström J M, L'Huillier A and Maquet A 2012 Introduction to attosecond delays in photoionization *J. Phys. B: At. Mol. Opt. Phys.* **45** 183001

[42] Friedrich H 1994 *Theoretical Atomic Physics* (Berlin: Springer)